Investigating the molecular mechanism of purslane-based vitiligo treatment using network pharmacology, molecular docking and *in vitro* analyses

XUEYING ZHANG[1], LELE MENG[1], XIAORONG RAN[1], SHUANG LI[1] and CHANGHUI WEN[2]

[1]The First Clinical College, Guizhou University of Traditional Chinese Medicine, Guiyang, Guizhou 550025, P.R. China; [2]Department of Dermatology, The First Affiliated Hospital of Guizhou University of Traditional Chinese Medicine, Guiyang, Guizhou 550001, P.R. China

Received October 23, 2024; Accepted February 10, 2025

DOI: 10.3892/mmr.2025.13482

Abstract. Purslane is a traditional Chinese medicine with a long-standing history of efficacy in the management of dermatological conditions such as vitiligo. However, the molecular mechanisms underlying its therapeutic effects on vitiligo remain unclear. Therefore, the present study explored these mechanisms using network pharmacology, molecular docking and *in vitro* experiments. Following the screening process, seven principal active components were identified, namely kaempferol, hesperetin, luteolin, quercetin, arachidonic acid, cycloartenol and β-sitosterol. In addition, six key targets, namely AKT1, tumor protein p53, peroxisome proliferator-activated receptor γ (PPARG), estrogen receptor 1, prostaglandin-endoperoxidase synthase 2 and mitogen-activated protein kinase 1, and eight pathways in purslane-based vitiligo treatment were identified. Network pharmacology and molecular docking demonstrated that flavonoids are the key components of purslane likely to mitigate oxidative stress damage in vitiligo. Gene Ontology and Kyoto Encyclopedia of Genes and Genomes enrichment analyses revealed that the phosphatidylinositol 3-kinase (PI3K)/AKT, p53 and PPARG signaling pathways are associated with purslane components and vitiligo. *In vitro* experiments revealed that purslane total flavones (PTF) increased cell viability, decreased ROS levels and increased antioxidant enzyme activities in H_2O_2-induced B16F10 cells. In addition, PTF activated the PI3K/AKT signaling pathway in H_2O_2-induced B16F10 cells, and the antioxidant effect of PTF was attenuated by a PI3K/AKT inhibitor. In conclusion, the findings of the present study suggest that the flavonoids of purslane contribute, at least in part, to its therapeutic effectiveness in vitiligo by mitigating oxidative stress in melanocytes through the PI3K/AKT signaling pathway.

Correspondence to: Professor Changhui Wen, Department of Dermatology, The First Affiliated Hospital of Guizhou University of Traditional Chinese Medicine, 71 Baoshan North Road, Yunyan, Guiyang, Guizhou 550001, P.R. China
E-mail: wenchanghui163@163.com

Abbreviations: PTF, purslane total flavones; DPPH, 1,1-diphenyl-2-trinitrophenylhydrazine; ROS, reactive oxygen species; SOD, superoxide dismutase; DCFH-DA, 2',7'-dichlorofluorescein diacetate; DAPI, 4',6-diamidino-2'-phenylindole; PPI, protein-protein interaction; GO, Gene Ontology; KEGG, Kyoto Encyclopedia of Genes and Genomes; PI3K, phosphatidylinositol 3-kinase

Key words: vitiligo, purslane, purslane total flavones, oxidative stress, reactive oxygen species, PI3K/AKT pathway

Introduction

Vitiligo is a common pigmentary disorder characterized by acquired localized or generalized skin depigmentation due to melanocyte dysfunction or loss (1). It presents a notable treatment challenge due to its propensity for relapse and resistance to treatment, and can be a mental and financial burden on patients and their families (2). The worldwide prevalence of vitiligo is estimated to be ~2% (3), with an increasing incidence in recent years, which has been suggested to be due to a fast-paced lifestyle and heightened psychological stress (4,5). Vitiligo can affect any area of the body, particularly exposed areas, and may lead to feelings of shame, anxiety and depression, with an impact on quality of life comparable to that of conditions such as psoriasis and eczema (2,6). Current western medicine therapies for vitiligo include oral or topical glucocorticoids, vitamin D3 analogs, immunosuppressants, surgical interventions and antioxidants (7). While these treatments demonstrate notable short-term efficacy, their long-term effectiveness is limited, often resulting in relapses and adverse reactions (8). This highlights the potential for research and development in traditional Chinese medicine, which is valued for its safety, affordability and minimal toxicity (9).

The etiology of vitiligo is unclear, with heredity, autoimmunity and environmental factors recognized as major contributors (10). Clinically, vitiligo manifests as depigmented patches on the skin or mucous membranes, with melanocytes as the primary targets of pathogenic mechanisms (11). Emerging evidence implicates oxidative stress in melanocyte depletion and dysfunction (7), suggesting that antioxidants from traditional Chinese medicine may aid in the management of vitiligo.

Purslane, known scientifically as *Portulaca oleracea* (L.), is an annual succulent herb, and its dried aerial parts are frequently used in the management of various dermatological conditions, including vitiligo, psoriasis, dermatitis and pruritus (12,13). The plant name has been verified using the World Flora Online database (www.worldfloraonline.org). Purslane has a rich historical background in the treatment of skin disorders, and is mentioned in ancient Chinese herbal texts such as the Compendium of Materia Medica, New Revision of Materia Medica, Dietary Materia Medica and Southern Yunnan Materia Medica. Pharmacological studies have identified numerous bioactive constituents in purslane, such as alkaloids, flavonoids, catecholamines and polysaccharides, that exhibit diverse pharmacological properties, including anti-inflammatory, antioxidant, analgesic, antibacterial and immunomodulatory effects (12,14).

Despite the extensive use of purslane in the management of vitiligo, the pharmacological mechanisms underlying its efficacy remain inadequately elucidated. Therefore, the present study utilized network pharmacology, molecular docking and *in vitro* experiments to comprehensively analyze the key active compounds of purslane, their targets and associated pathways in the context of vitiligo treatment. The present study aims to establish a theoretical basis for understanding the therapeutic mechanisms of purslane in the treatment of vitiligo, and to provide new perspectives for clinical research into this natural product.

Materials and methods

Network pharmacology

Collection and screening of active ingredients of purslane. The Traditional Chinese Medicine Systems Pharmacology Database (TCMSP; http://tcmspw.com/tcmsp.php/) was utilized to compile all bioactive compounds of purslane (15). Active ingredients meeting the criteria of oral bioavailability ≥30%, drug-likeness ≥0.1, molecular weight ≤500, hydrogen bond donors ≤5, hydrogen bond acceptors ≤10 and fat-water partition coefficient ≤5 were identified as the principal bioactive constituents of purslane (16).

Screening of potential targets for the main active components of purslane. The primary bioactive compounds identified from the TCMSP database were cross-referenced with the PubChem database (https://pubchem.ncbi.nlm.nih.gov) to identify known protein targets and map protein names to their respective gene names (17). In addition, the Swiss Target Prediction database (http://www.swisstargetprediction.ch/) was used to predict potential targets of the main bioactive constituents, with P>0 for target prediction (18). The potential targets obtained from the PubChem and Swiss Target Prediction databases were integrated, de-duplicated and regarded as the potential targets of the primary bioactive compounds of purslane.

Screening of potential targets for vitiligo. The GeneCards database (https://www.genecards.org/) (19) and DisGeNET database (https://www.disgenet.org/) (20) were searched using the keyword 'vitiligo' to identify disease-related targets. The targets identified from the two databases were consolidated to obtain the potential targets associated with vitiligo.

Screening of potential targets of purslane in the treatment of vitiligo. The potential targets of the primary bioactive compounds of purslane were compared with the potential targets associated with vitiligo and entered into the Microscopic Letter platform (http://www.bioinformatics.com.cn/) for analysis. An intersection map was created to identify the potential targets of purslane for the management of vitiligo (21).

Construction of a purslane active ingredient-target network. The bioactive constituents of purslane and their potential targets for the treatment of vitiligo were imported into Cytoscape version 3.7.2 software (22) to generate a drug component-potential target network for purslane in the context of vitiligo treatment. In this network, each node represents an active ingredient or a potential target, while each edge denotes the interaction between the bioactive compound and the potential target. Subsequently, the Cytoscape plug-in CytoNCA version 2.1.6 was used to analyze the topological properties of the network (23). Metrics such as betweenness centrality (BC), closeness centrality (CC), and degree centrality (DC) were calculated to identify the primary bioactive compounds of purslane that may be useful for vitiligo treatment. In network pharmacology, the calculation of BC, CC and DC values is primarily employed to identify key nodes within the network, assess the efficiency of information transfer among nodes and uncover the network's core regulatory mechanisms. This analytical approach facilitates drug target prediction, enhances the design of multi-target drugs and improves the overall comprehensiveness of network analysis, thereby providing a robust theoretical foundation for drug discovery and disease treatment (23).

Construction of a protein-protein interaction (PPI) network. The potential targets of purslane for the treatment of vitiligo were uploaded to the STRING database (https://string-db.org) (24) to generate a PPI network. The analysis was performed by choosing 'Multiple proteins' to integrate the overlapping genes of purslane and vitiligo, designating '*Homo sapiens*' as the organism, configuring the 'Minimum required interaction score' to medium confidence (0.400), and maintaining default settings for other parameter options to produce the PPI network. The resulting data were imported into Cytoscape version 3.7.2 software for visualization of the PPI network. Subsequently, the topological properties of the network were analyzed using the Cytohubba 0.1 plug-in in Cytoscape. Key metrics, including Degree, Edge Percolated Component (EPC), Maximum Neighborhood Component (MNC), Maximal Clique Centrality (MCC), Betweenness and Closeness, were calculated to identify potential key targets of purslane for the treatment of vitiligo (25).

Gene Ontology (GO) enrichment analysis and Kyoto Genes and Genomes (KEGG) pathway enrichment analysis of potential targets. The potential target genes associated with the purslane treatment of vitiligo were analyzed for GO enrichment and KEGG pathway enrichment using the DAVID database (https://david.ncifcrf.gov) (26). The analysis was performed by inputting the overlapping gene list between purslane and vitiligo, using 'OFFICIAL_GENE_SYMBOL' as the identifier, '*Homo sapiens*' as the species and 'Gene list' as the list type, and submitting the list for annotation. P<0.002 was applied as the cutoff for GO annotation and KEGG pathway enrichment analysis (27).

Molecular docking. Molecular docking of the key constituents of purslane with the key targets was performed. The 3-dimensional (3D) crystal structures of the target proteins were obtained from the RCSB Protein Data Bank (PDB) database (https://www.rcsb.org) to act as the receptors. Using PyMol version 2.2.0 software, the target proteins were dehydrated, non-relevant ligands were removed, and the results were saved in standard PDB format (28). The 3D structures of the compounds were acquired from the TCMSP database and saved in mol2 format. OpenBabel version 2.4.1 (http://openbabel.org) was used to convert the 3D structure file format to a PDB format file (29).

AutoDockTools version 1.5.7 was used to add hydrogen atoms to the target proteins and calculate their charges. Then AutoDockTools version 1.5.7 Vina software was applied to dock the receptor protein with the ligand and calculate the binding energy (30). Following this, PyMol version 2.2.0 was used to visualize the docking outcomes.

Experimental verification

B16F10 cell culture. B16F10 mouse melanoma cells (cat. no. CX0109) were acquired from Wuhan Boster Biological Technology, Ltd. The cells were verified to be free of *Mycoplasma* contamination. In addition, the B16F10 cells were identified by STR analysis as a subline of B16-F0 cells. The cells were cultured in RPMI-1640 complete medium (cat. no. C11875500BT; Gibco; Thermo Fisher Scientific, Inc.) containing 10% fetal bovine serum (cat. no. FSP500; Shanghai ExCell Biology, Inc.) in a CO_2 incubator at 37˚C with 5% CO_2. The culture medium was replenished every 2 days (31).

Purslane total flavonoids (PTF) dosage screening. B16F10 cells in the logarithmic growth phase were plated in 96-well plates at a density of $5x10^3$ cells per well. Subsequently, 100 μl PTF medium containing different concentrations of PTF (0, 10, 20, 40, 80, 160, 320, 640 and 1,280 μg/ml) was added to each well. The medium was prepared by dissolving PTF (purity ≥80%; MF2023115; Mufan Biotechnology Co., Ltd.) in dimethyl sulfoxide (DMSO; Beijing Solarbio Science & Technology Co., Ltd.) and diluting the solution to the desired concentration in the medium before use, ensuring the final concentration of DMSO was <0.2%. Each group comprised 6 replicate wells and cultured in an incubator at 37˚C with 5% CO_2 for 24 h. After incubation, 10% Cell Counting Kit-8 (CCK-8) reagent [cat. no. C6005; UElandy (Suzhou) Co., Ltd.] was added to each well. Following incubation for 1-2 h, the absorbance (A) value at 450 nm was measured using a Synergy 2 microplate reader (BioTek; Agilent Technologies, Inc.). Subsequently, the cell viability was calculated using the following formula: Cell viability (%)=$(A_{control}-A_{blank})/(A_{drug}-A_{blank})$ (32).

Evaluation of 1,1-diphenyl-2-trinitrophenylhydrazide (DPPH) free radical scavenging ability. PTF solution of various concentrations (10, 20, 40, 80, 160, 320, 640 and 1,280 μg/ml) was mixed with 1.0 ml of 200 μM DPPH (cat. no. D273092; Shanghai Aladdin Biochemical Technology Co., Ltd.) in ethanol. The ethanolic DPPH solution was used as a control, and the reaction between PTF and DPPH was carried out at 37˚C for 60 min, followed by colorimetric measurement at a wavelength of 517 nm. The DPPH radical scavenging activity was calculated using the following formula: DPPH (%)=$1-[(A_{blank}-A_{sample})/A_{blank}]$ x100 (33).

Effect of PTF on oxidative stress injury in B16F10 melanocytes. Cells in the logarithmic growth phase were harvested and counted after digestion with 0.25% trypsin solution (C25200056; Gibco; Thermo Fisher Scientific, Inc.) and the cells were centrifuged at 400 x g for 5 min using a high-speed refrigerated centrifuge (D3024R; Dalong Xingchuang Experimental Instrument (Beijing) Co., Ltd,). The cell concentration was adjusted to $5x10^3$ cells/100 μl, and 100 μl cell suspension was seeded into each well of a 96-well plate. The cells were then cultured for 24 h at 37˚C in a 5% CO_2 incubator, after which the culture medium was removed. The control group was incubated with RPMI-1640 medium alone, while the drug intervention groups were exposed to RPMI-1640 medium supplemented with varying concentrations of PTF (40, 80, 160, 320 and 640 μg/ml) cultured in an incubator at 37˚C with 5% CO_2 for 2, 4 and 6 h. Following this, 500 μM hydrogen peroxide (H_2O_2; cat. no. 20230726; Tianjin Damao Chemical Reagent Co., Ltd.) was added to each well and the plate was incubated cultured in an incubator at 37˚C with 5% CO_2 for an additional 24 h (34). Subsequently, 10% CCK-8 reagent was added to each well to assess cell viability using the aforementioned protocol.

Detection of oxidative stress levels in cells. B16F10 cells were plated in 12-well plates at a density of $5x10^5$ cells per well. The cells were treated with PTF (40, 80 and 160 μg/ml) or extract of *Ginkgo biloba* (EGB; 10:1 purification, water extract; cat. no. G195711-25g; Shanghai Aladdin Biochemical Technology Co., Ltd.) for 2 h, followed by 500 μM hydrogen peroxide for 24 h as described above. In addition, in certain wells, the B16F10 cells were pretreated with the 20 μmol/l PI3K inhibitor LY294002 for 2 h (cat. no. S1737-1mg; Beyotime Institute of Biotechnology) prior to the 160 μg/ml PTF and H_2O_2 treatments. The medium was aspirated, and the DCFH-DA probe from a Reactive Oxygen Species (ROS) Detection kit (cat. no. S0033S; Beyotime Institute of Biotechnology) was applied at 1:1,000 dilution. The cells were then incubated with the probe for 20 min under standard culture conditions (37˚C, 5% CO_2), rinsed with PBS and visualized using a 488-nm excitation long-wave microscope (35). The superoxide dismutase (SOD) and catalase (CAT) activity and melanin content in the cells were measured using specific kits, and the results were determined using a microplate reader. The kits were as follows: Total SOD Activity Detection Kit, WST-8 method (cat. no. S0101S; Beyotime Institute of Biotechnology), Catalase Detection Kit (cat. no. S0051; Beyotime Institute of Biotechnology) and Mouse Melanin (MC) ELISA Research Kit (cat. no. MM-0870M2; Shanghai Enzyme-linked Biotechnology Co., Ltd.) (36).

Western blotting. B16F10 cells from each experimental group were harvested, homogenized with RIPA Lysis and Extraction Buffer (cat. no. 89900; Thermo Fisher Scientific, Inc.) with phenylmethylsulfonyl fluoride (100 mM; cat. no. P0100-1ml; Beijing Solarbio Science & Technology Co., Ltd.), and then subjected to lysis on ice for 30 min. The supernatant was collected for subsequent analysis. The protein concentration was quantified using a BCA Protein Concentration Assay Kit (500X dilution; cat. no. P0012, Beyotime Institute of Biotechnology). After mixing with buffer, protein denaturation was carried out in a water bath at 100˚C for 10 min. The precast gel (4-12%

Table I. Main active components of purslane.

Compound	Molecular weight	Drug likeness	Oral bioavailability, %	MolID
Kaempferol	286.25	0.24	41.88	MOL000422
Hesperetin	302.3	0.27	47.74	MOL005100
Luteolin	286.25	0.25	36.16	MOL000006
Isobetanidin	388.36	0.52	59.73	MOL006657
Isobetanin_qt	388.36	0.52	30.16	MOL006662
Quercetin	302.25	0.28	46.43	MOL000098
Arachidonic acid	304.52	0.2	45.57	MOL001439
Cycloartenol	426.8	0.78	38.69	MOL003578
β-carotene	536.96	0.58	37.18	MOL002773
β-sitosterol	414.79	0.75	36.91	MOL000358

MolID, molecular ID from The Traditional Chinese Medicine Systems Pharmacology Database.

Bis-Tris prefabricated glue; cat. no. WBT41212BOX; Thermo Fisher Scientific, Inc.) was secured in an electrophoresis chamber, and electrophoresis buffer was added to the reservoir. The protein samples and marker (20-120 kDa marker, cat. no. M00521, GenScript Biotech Corporation; 10-250 kDa marker, cat. no. MF028-plus-01, Mei5 Biotechnology Co., Ltd.) were loaded into the wells at a total protein content of 40 μg/lane. The gel was subjected to electrophoresis at a constant voltage of 180 V until the bromophenol blue dye front reached the bottom of the gel, typically 40 min. Subsequently, the cells were transferred to a PVDF membrane (cat. no. ISEQ15150; Merck KGaA), which was then blocked with 5% skimmed milk powder for 2 h at room temperature. After washing with Tris-buffered saline with 0.1% Tween 20, the PVDF membranes were incubated with primary antibodies targeting β-actin (1:30,000; cat. no. 66009-1-Ig; Wuhan Sanying Biotechnology), GAPDH (1:30,000; cat. no. 60004-1-Ig; Wuhan Sanying Biotechnology), AKT (1:2,000; cat. no. 10176-2-AP; Wuhan Sanying Biotechnology), phosphorylated (p-)AKT (1:1,000; cat. no. 4060; Cell Signaling Technology, Inc.), Bax (1:8,000; cat. no, 50599-2-Ig; Wuhan Sanying Biotechnology) and Bcl-2 (1:2,000; cat. no, 26593-1-AP; Wuhan Sanying Biotechnology) overnight at 4˚C. The following day, HRP was used to label sheep anti-rabbit or sheep anti-mouse secondary antibody (1:10,000; cat. nos. BA1054 or BA1051; Wuhan Boster Biological Technology, Ltd.) was applied and the membrane was incubated for 2 h at room temperature on a shaker. ECL reagent (cat. no. KF8003, Affinity Biosciences) was then used to treat the PVDF membrane, which was subjected to automatic exposure. If the bands were not clearly visible or did not appear, manual exposure was performed using chemiluminescence imaging system for color development (model SH-523; Hangzhou Shenhua Technology Co., Ltd.). Image J software (version 1.8.0, National Institutes of Health) was used to analyze the gray values of protein bands.

Immunofluorescence detection. B16F10 cells were cultured in 24-well plates. After drug treatment, the culture medium was removed, and the cells were fixed with 4% paraformaldehyde at 25˚C for 30 min and permeabilized with 5% Triton X-100 (cat. no. ST795; Beyotime Institute of Biotechnology). The cells were subsequently incubated at 37˚C for 30 min and blocked with 10% goat serum at room temperature for 1 h (cat. no. AR1009; Boster Biological Technology). Primary antibodies against melan-A (1:100; cat no. SC56-02; HUABIO) were added and the samples were incubated overnight at 4˚C. Melan-A is the most used indicator to detect the presence and delineate the distribution of melanocytes in skin pathology (37). The next day, sheep anti-rabbit secondary antibody (BA1032; Boster Biological Technology Co. Ltd.) was applied in the dark. Following 1 h incubation at room temperature, the cells were stained with 4',6-diamidino-2'-phenylindole (C1002; Beyotime Institute of Biotechnology) in the dark for 5 min to visualize the nuclei. The stained samples were then observed under a fluorescence microscope.

Statistical analysis. Statistical analysis and graphical representation were performed using GraphPad Prism 9.0 software (Dotmatics). Data are presented as the mean ± standard error of the mean. All experiments were performed in triplicate at least to ensure the reproducibility of the experimental results. Statistical analysis was performed using one-way analysis of variance followed by Dunnett's or Tukey's post hoc tests to assess differences among multiple groups. When Tukey's test was performed, only some significant differences are shown for clarity. $P \leq 0.05$ was considered to indicate a statistically significant difference.

Results

Major active components and targets of purslane. In total, 54 chemical components of purslane were extracted from the TCMSP database. Following screening, 10 candidate compounds were identified as the principal active constituents. These were kaempferol, hesperetin, luteolin, isobetanidin, isobetanin_qt, quercetin, arachidonic acid, cycloartenol, β-carotene and β-sitosterol (Table I).

Analysis using the Swiss Target Prediction database platform led to the identification of a total of 563 targets with $P>0$. Among these, 92 targets were associated with hesperetin, 100 with arachidonic acid, 44 with β-sitosterol, 1 with β-carotene,

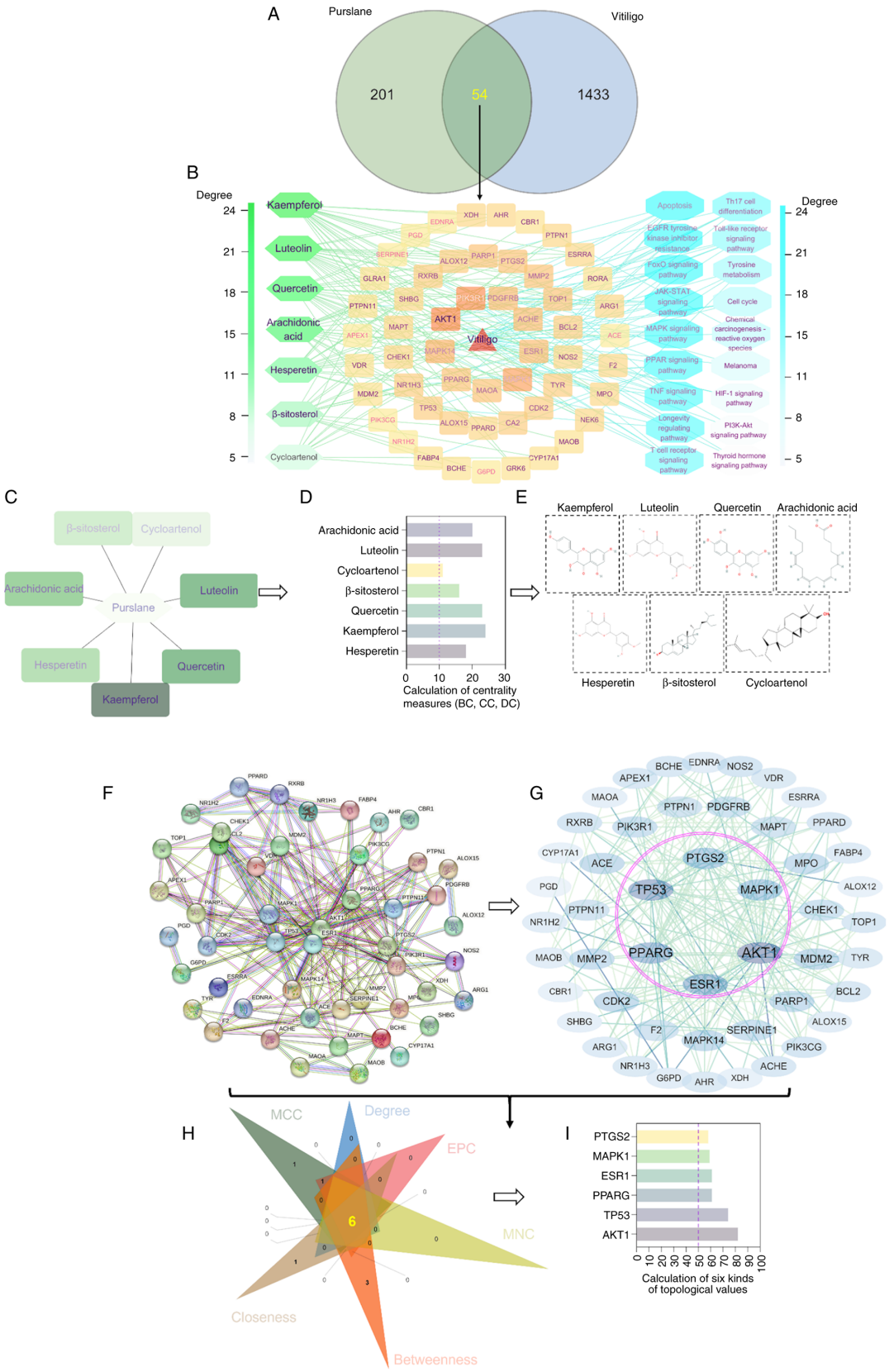

Figure 1. Pharmacological screening of the target network associated with the use of purslane for vitiligo treatment. (A) Venn diagram illustrating intersecting targets associated with purslane and vitiligo. (B) Network diagram of purslane active components, their gene targets and target pathways. (C) Core active components of purslane. (D) Utilization of the CytoNCA plugin in Cytoscape to select and quantify the core ingredients of purslane. (E) Chemical structures of the active components of purslane. Screening of the key targets of purslane in vitiligo treatment was performed. (F) Protein-protein interaction network comprising key targets of purslane in vitiligo treatment and (G) Cytohubba analysis. Nodes represent targets, and edges represent interactions between targets. Nodes with larger font and darker color indicate higher degree values, signifying a greater impact on vitiligo. (H) Six algorithms, namely degree, MCC, EPC, MNC, betweenness and closeness, were utilized to identify core targets. (I) Quantification of the core targets of purslane in the treatment of vitiligo. MCC, maximal clique centrality; EPC, edge percolated component; MNC, maximum neighborhood component; PTGS2, prostaglandin-endoperoxidase synthase 2; MAPK1, mitogen-activated protein kinase 1; ESR1, estrogen receptor 1; PPARG, peroxisome proliferator-activated receptor γ; TP53, tumor protein p53.

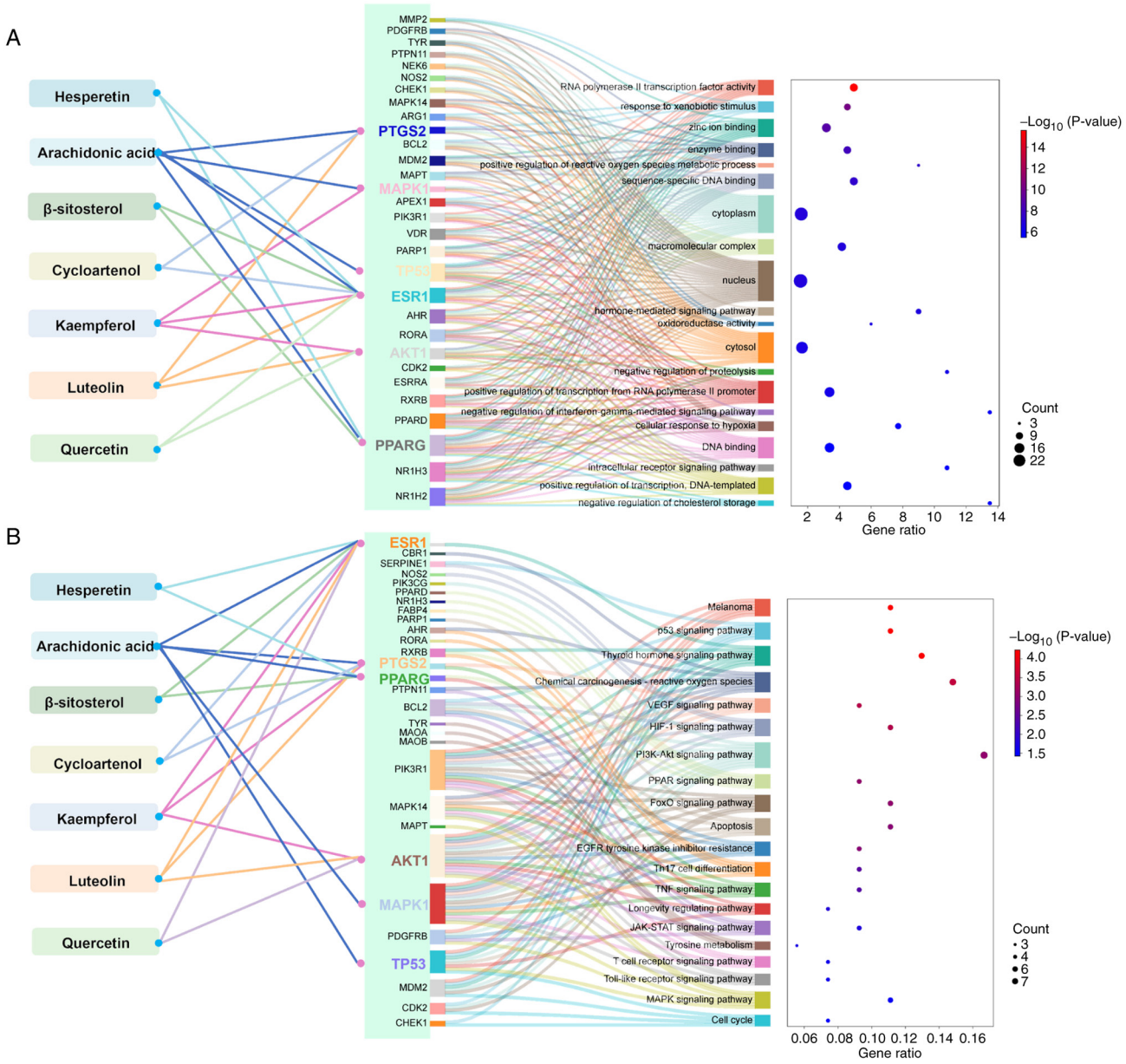

Figure 2. Target enrichment analysis of purslane in vitiligo treatment. (A) GO enrichment analysis of core targets of purslane components in vitiligo treatment. Core components are on the left, core targets in the middle and GO terms on the right. (B) KEGG enrichment analysis of core targets of purslane components in vitiligo treatment: Core components are on the left, core targets in the middle and KEGG pathways on the right. In both panels, red and green colors indicate distinct P-value thresholds, and dot size reflects the number of genes associated with each term. GO, Gene Ontology; KEGG, Kyoto Encyclopedia of Genes and Genomes; PTGS2, prostaglandin-endoperoxidase synthase 2; MAPK1, mitogen-activated protein kinase 1; ESR1, estrogen receptor 1; PPARG, peroxisome proliferator-activated receptor γ; TP53, tumor protein p53.

25 with cycloartenol, 2 with isobetanidin, 12 with kaempferol, 100 with luteolin and 100 with quercetin. Through the integration of all targets obtained from the database screening process and the elimination of duplicate or invalid targets, a total of 255 targets associated with the primary active components of purslane were obtained (Table SI).

Main component-target gene-signaling pathway network of purslane for vitiligo treatment. A total of 1,736 vitiligo-related targets were identified through searches in the DisGeNet and GeneCards databases. Following the elimination of duplicate targets, 1,487 unique vitiligo targets were obtained. By intersecting the targets of the active components in purslane with the known disease-related targets of vitiligo, 54 common targets were identified as potential targets for purslane in the treatment of vitiligo (Fig. 1A). Subsequently, a network illustrating the relationships between the active components of purslane and the associated target genes for the treatment of vitiligo was constructed, comprising 54 potential targets and seven active components (Fig. 1B). This network comprised 64 nodes and 137 edges, with an average BC of 118.59, CC of 0.355 and DC of 4.28. Notably, the seven active components kaempferol, hesperetin, luteolin, quercetin, arachidonic acid, cycloartenol and b-sitosterol had BC, CC and DC values exceeding the network average (Fig. 1C-E), suggesting their potential as key active components of purslane in the treatment

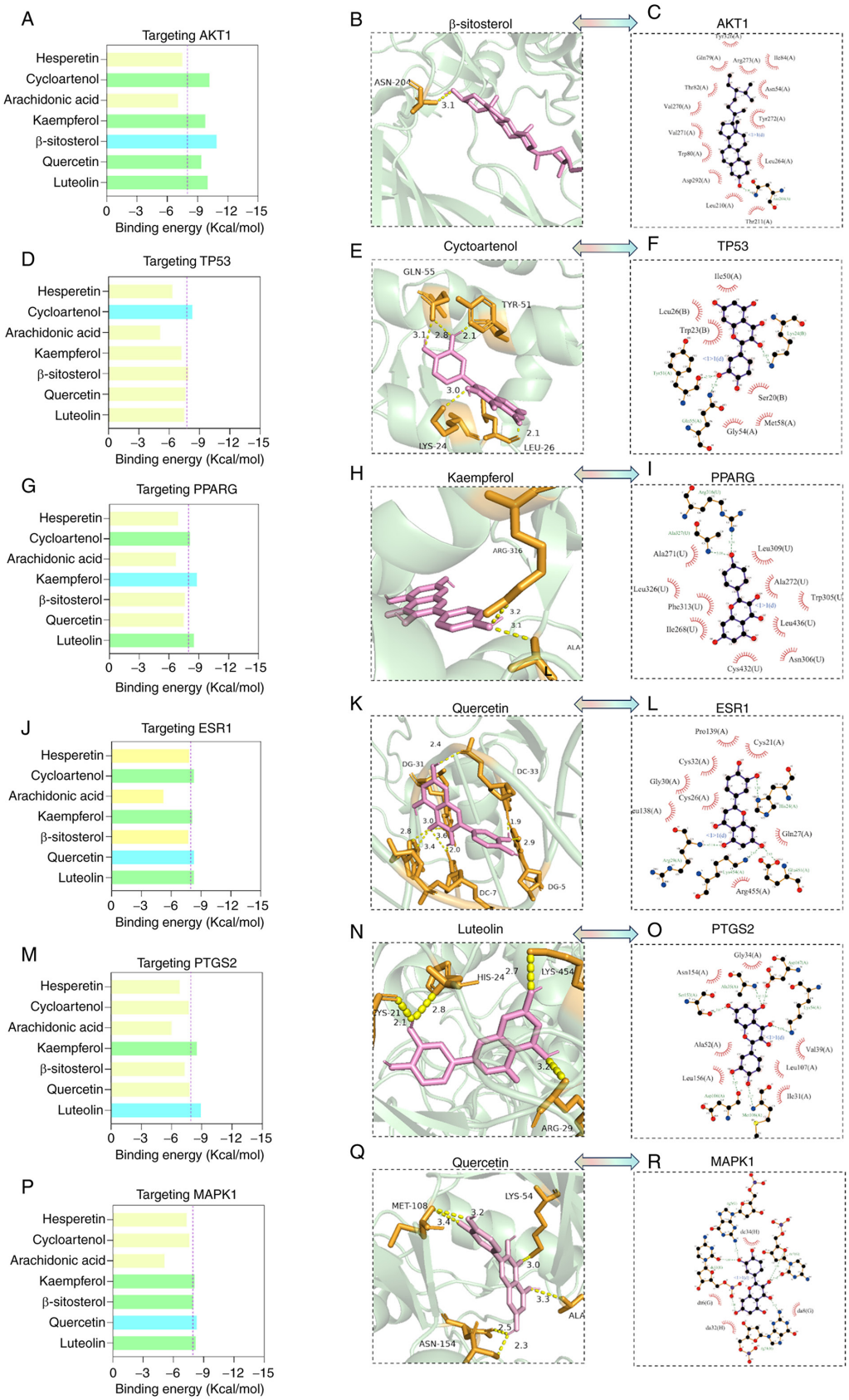

Figure 3. Molecular docking of purslane core components with core targets. (A-F) Binding free energies of core components and core targets. Blue columns represent the constituents with the lowest binding free energy, yellow columns indicate those with binding free energy >-8 kJ/mol and green columns indicate those with binding free energy <-8 kJ/mol. (G-L) Schematic 3-dimensional structures show the docking of core components with core target molecules. The pink molecular structures depict the core components of purslane, the orange structures represent amino acid residues that directly interact with the components, and yellow dotted lines signify hydrogen bonds formed between the components and amino acid residues. (M-R) Two-dimensional representation of the interaction of the core components of purslane with protein targets, where hydrogen bonds are green dashed lines and hydrophobic interactions are red radial arcs. PTGS2, prostaglandin-endoperoxidase synthase 2; MAPK1, mitogen-activated protein kinase 1; ESR1, estrogen receptor 1; PPARG, peroxisome proliferator-activated receptor γ; TP53, tumor protein p53.

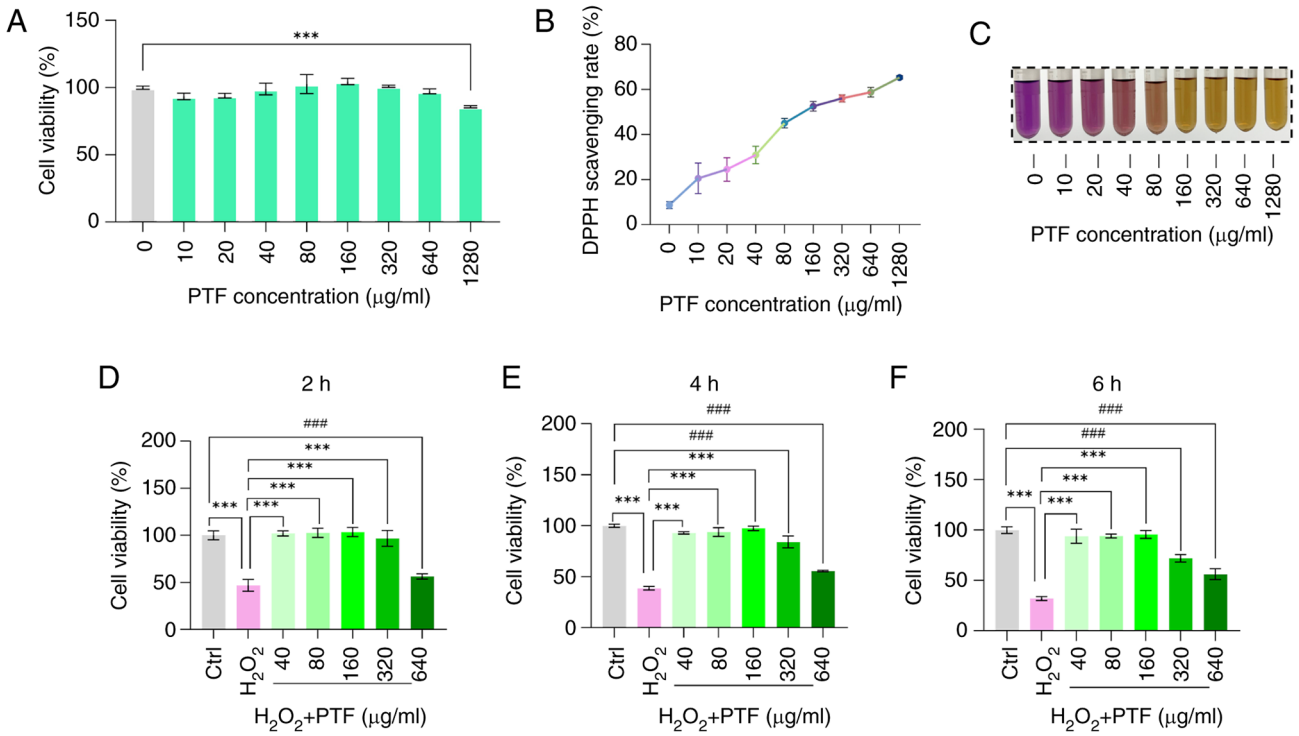

Figure 4. Dose screening of PTF in B16F10 cells. (A) Effects of different concentrations of PTF on the viability of B16F10 cells. (B) Quantitative analysis of the free radical scavenging rate of different doses of PTF and (C) representative images from the DPPH assay. Antioxidant activity of different doses of PTF on B16F10 cells at (D) 2 h, (E) 4 h and (F) 6 h after H_2O_2 treatment. Data are presented as the mean ± standard error of the mean. ###P<0.001 vs. the Ctrl group; ***P<0.001 vs. the H_2O_2 group. PTF, purslane total flavonoids; DPPH, 1,1-diphenyl-2-trinitrophenylhydrazine; Ctrl, control; H_2O_2, hydrogen peroxide.

of vitiligo and offering valuable insights for future studies. Moreover, a PPI network was generated, comprising 49 nodes and 230 edges. Cytohubba analysis highlighted six key targets, namely AKT1, tumor protein p53 (TP53), peroxisome proliferator-activated receptor γ (PPARG), estrogen receptor 1 (ESR1), prostaglandin-endoperoxidase synthase 2 (PTGS2) and mitogen-activated protein kinase 1 (MAPK1), which are suggested to be important as potential targets of purslane in the treatment of vitiligo (Fig. 1F-I).

GO functional enrichment analysis indicated that the use of purslane in vitiligo treatment may potentially influence 'DNA binding' and various cellular functions. This is potentially mediated via the effects of arachidonic acid, kaempferol, luteolin and quercetin on key genes, namely AKT1, ESR1, PPARG, PTGS2, MAPK1 and TP53, by modulating the processes 'cellular response to hypoxia', 'enzyme binding' and 'zinc ion binding', by affecting the cellular components 'cytosol' and 'nucleus', as well as 'response to xenobiotic stimulus' (Fig. 2A).

KEGG pathway enrichment analysis revealed that the targeting of ESR1 and PPARG by hesperetin could potentially influence the 'thyroid hormone signaling pathway', 'PPAR signaling pathway' and 'longevity regulating pathway' in the context of vitiligo treatment. Additionally, arachidonic acid was suggested to impact 'melanoma' and 'VEGF signaling pathway' by targeting ESR1, PTGS2, PPARG, MAPK1 and TP53. Furthermore, kaempferol and luteolin were indicated to act on ESR1, PTGS2 and AKT targets, demonstrating therapeutic effects on vitiligo through modulation of the 'PI3K-Akt signaling pathway', 'p53 signaling pathway' and 'PPAR signaling pathway' (Fig. 2B).

Overall, the screening process led to the identification of 7 principal components, namely kaempferol, hesperetin, luteolin, quercetin, arachidonic acid, cycloartenol and β-sitosterol, from 54 potential ingredients, in addition to 6 key targets, namely AKT1, TP53, PPARG, ESR1, PTGS2 and MAPK1, from 54 potential targets, and 8 pathways from 20 potential pathway for purslane-based vitiligo treatment.

Molecular docking of purslane core components with core targets. Utilizing the findings from the PPI network and the purslane component-target gene network analyses, AKT1 (7nh5), TP53 (1ycq), PPARG (1fm6), ESR1 (1hcq), PTGS2 (P35354) and MAPK1 (P28482) were selected as candidate macromolecules for further investigation. The binding energy of these proteins with the corresponding active compounds was evaluated. The analysis suggested that b-sitosterol could form a hydrogen bond with the Asn-204 residue of AKT1 with a binding energy of -10.9 kcal/mol (Fig. 3A and B). In addition, it suggested that cycloartenol could form hydrogen bonds with the Gln-55, Tyr-51, Lys-24 and Leu-26 residues of TP53 with a binding energy of -7.9 kcal/mol (Fig. 3D and E); kaempferol could form hydrogen bonds with the Arg-316 and Ala-327 residues in PPARG with a binding energy of -8.8 kcal/mol (Fig. 3G and H); and luteolin could form hydrogen bonds with the Cys-21, His-24, Lys-454 and Arg-29 residues of PTGS2 with a binding energy of -8.5 kcal/mol (Fig. 3M and N). In addition, quercetin was predicted to form hydrogen bonds with the diacylglycerol (DG)-31, dicarboxylic acid (DC)-7, DG-5

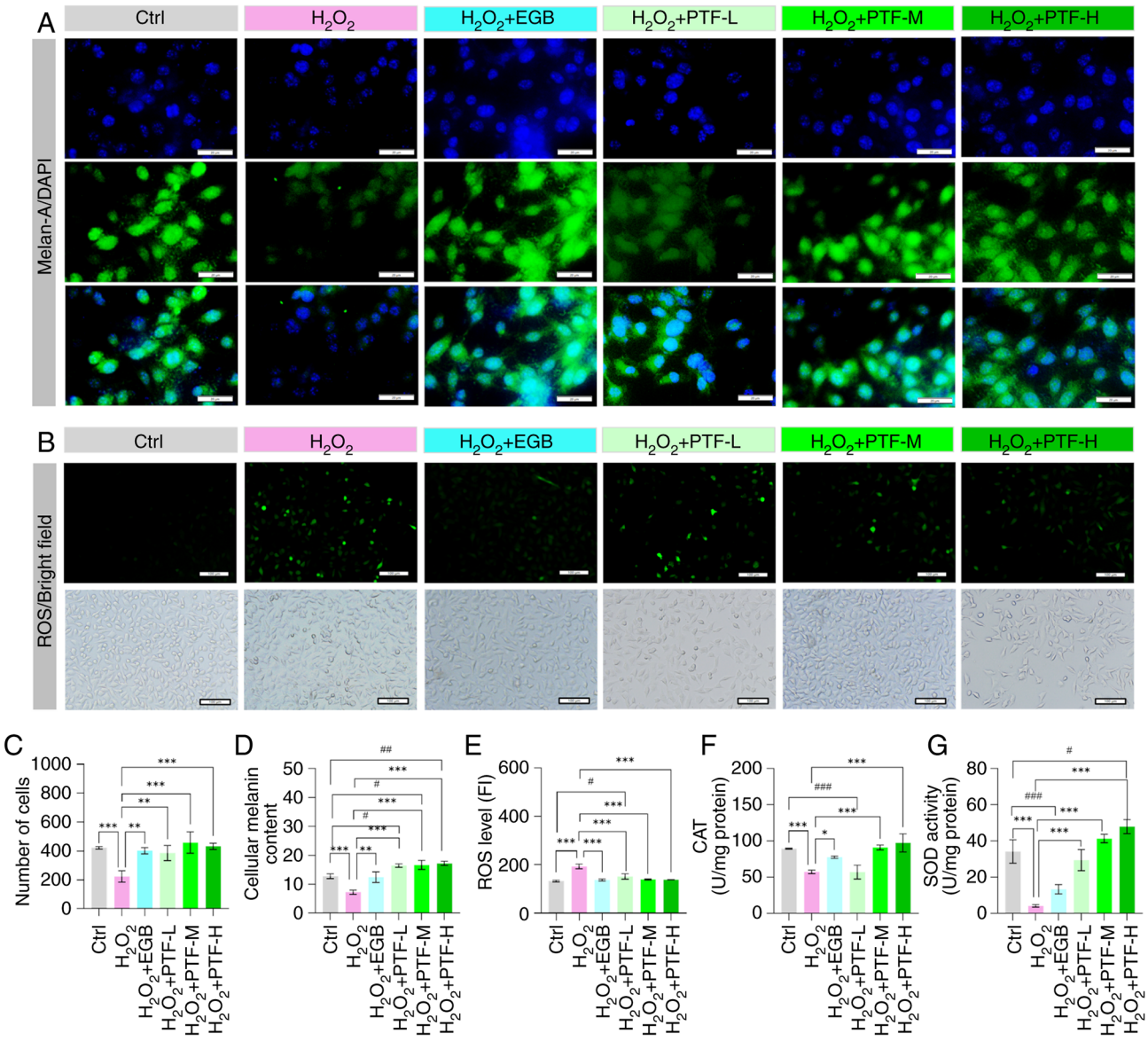

Figure 5. Protective effect of PTF against H_2O_2 -induced oxidative damage in B16F10 cells. (A) Effect of different treatments on melan-A protein expression in B16F10 cells (scale bar, 20 μm). Green signals represent the staining of melan-A with a melanocyte-specific antibody, and blue signals represent DAPI. (B) Effects of different treatments on the ROS content of B16F10 cells (scale bar, 100 μm). Quantification of (C) the numbers of cells positive for melan-A and (D) melanin content in B16F10 cells. Quantification of the (E) ROS content, (F) CAT activity and (G) SOD activity in the B16F10 cells. All data are presented as the mean ± standard error of the mean. $^{\#}$P<0.05, $^{\#\#}$P<0.01 and $^{\#\#\#}$P<0.001 vs. the Ctrl group; *P<0.05, **P<0.01 and ***P<0.001 vs. the H_2O_2 group. PTF, purslane total flavonoids; H_2O_2, hydrogen peroxide; Ctrl, control; DAPI, 4',6-diamidino-2'-phenylindole; ROS, reactive oxygen species; CAT, catalase; SOD, superoxide dismutase; EGB, extract of *Ginkgo biloba*; L, low; M, medium; H, high; FI, fluorescence intensity.

and DC-33 residues of ESR1 with a binding energy of -8.3 kcal/mol (Fig. 3J and K), and with the Met-108, Lys-54, Ala-35 and Asn-154 residues of MAPK1 with a binding energy of -7.8 kcal/mol (Fig. 3P and Q). Hydrogen bonding and hydrophobic interactions between the purslane core components and the selected targets are presented in (Fig. 3C, F, I, L, O and R). These findings suggest that flavonoids are the predominant components of purslane that interact with vitiligo-associated targets.

Total flavonoids of purslane alleviate oxidative stress impairment in B16F10 cells. To investigate the protective effects of PTF against oxidative stress, *in vitro* experiments were conducted. Initially, a CCK-8 assay was utilized to determine the optimal concentration of PTF. Results indicated that interventions of 10-640 μg/ml had no significant impact on B16F10 cell viability. However, an increase in concentration to 1,280 μg/ml resulted in a significant reduction in B16F10 cell viability and notable cytotoxicity (Fig. 4A).

The DPPH assay was then employed to evaluate the antioxidant effect of PTF. This assay assesses the ability of antioxidants to scavenge DPPH free radicals by monitoring changes in absorbance. The results revealed that antioxidant effect increased as the PTF concentration increased (Fig. 4B and C).

To investigate the antioxidative effect of PTF on H_2O_2-induced oxidative stress in B16F10 cells, the cells were treated with H_2O_2 (500 μM) to establish an oxidative stress

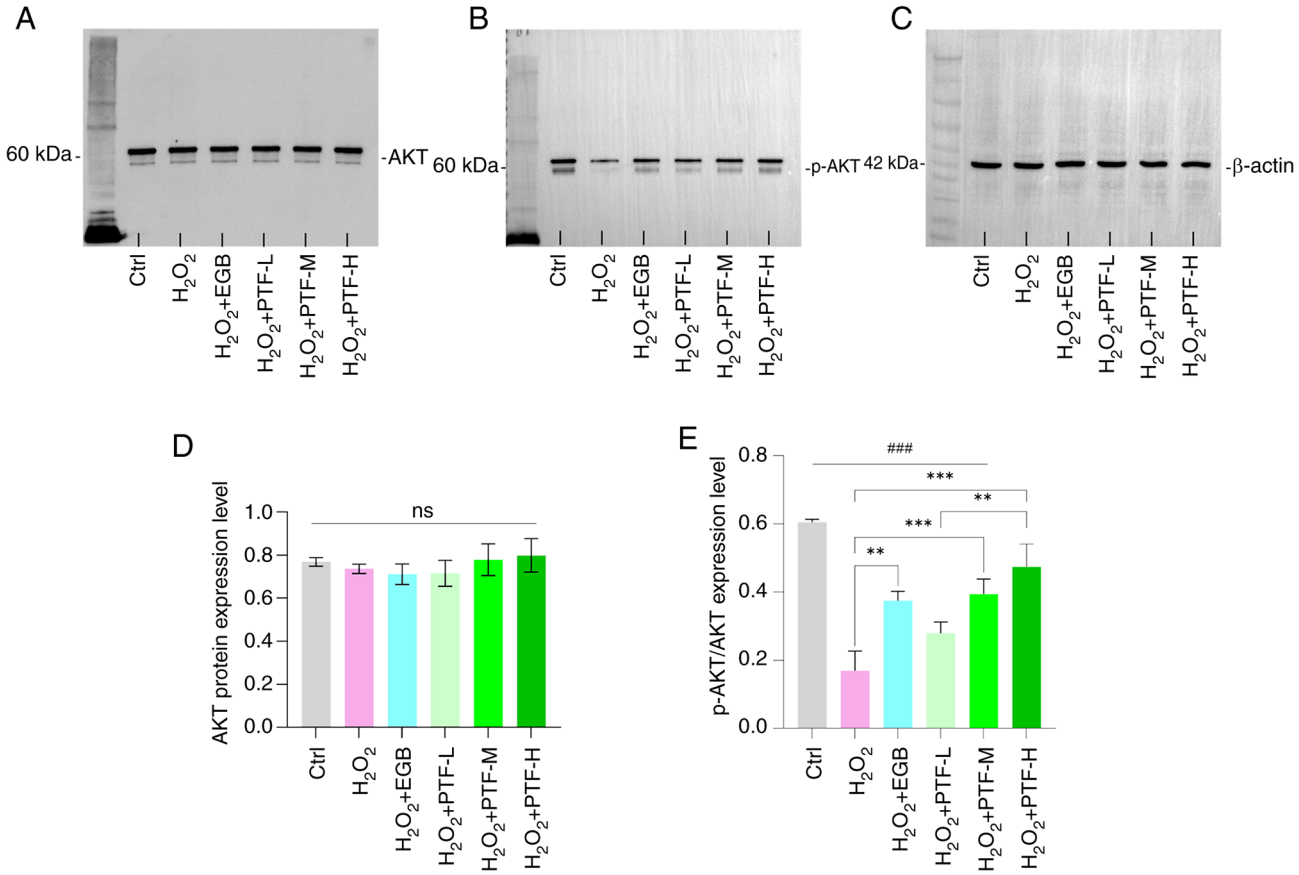

Figure 6. PTF activates AKT signaling in B16F10 cells stimulated with H_2O_2. Western blot analysis of (A) AKT, (B) p-AKT and (C) β-actin internal control. Quantitative analysis of (D) AKT expression and (E) p-AKT protein levels. All data are presented as the mean ± standard error of the mean. $^{###}$P<0.001 vs. the Ctrl group; **P<0.01 and ***P<0.001 vs. the H_2O_2 group. PTF, purslane total flavonoids; H_2O_2, hydrogen peroxide; Ctrl, control; p-, phosphorylated; EGB, extract of *Ginkgo biloba*; L, low; M, medium; H, high.

model. The cells were pretreated with various concentrations of PTF (40, 80, 160, 320 and 640 μg/ml) prior to treatment with H_2O_2 for 24 h. Results revealed that following H_2O_2 treatment, the viability of the B16F10 cells significantly decreased compared with that of the control cells. However, preincubation with PTF at concentrations of 40, 80 and 160 μg/ml for 2, 4 and 6 h significantly increased cell viability compared with that of the model group. By contrast, the cell survival rate decreased significantly in cells preincubated with 320 and 640 μg/ml PTF for 4 and 6 h compared with that in the control group (Fig. 4D-F). Consequently, PTF concentrations of 40, 80 and 160 μg/ml were selected for use in subsequent experiments, in which they were referred to as the low, medium and high PTF, respectively.

To examine the protective effect of PTF against H_2O_2-induced oxidative damage, the B16F10 cells were incubated with various concentrations of PTF or 100 μg EBG for 2 h prior to treatment with 500 μM H_2O_2 for 24 h, and melan-A fluorescence levels, melanin content, SOD and CAT activity and ROS levels were then measured. The results demonstrate that the melan-A fluorescence intensity and melanin content were significantly reduced in the H_2O_2 model group compared with that in the control group. Conversely, the melan-A fluorescence intensity and melanin content were significantly elevated in the EGB and various PTF dose groups compared with those in the model group (Fig. 5A, C and D). The ROS level in the H_2O_2 model group was significantly elevated compared with that in the control group, whereas the CAT and SOD levels were significantly reduced. Following intervention with different doses of PTF and EGB, the ROS levels were significantly decreased compared with those in the H_2O_2 model group, with no significant difference observed among the low, medium and high PTF concentration groups. In addition, significant increases in the activity levels of CAT in the medium and high PTF and EGB groups, and of SOD in all PTF groups were observed compared with those in the model group. Furthermore, as the PTF concentration increased, the activity levels of CAT and SOD also increased. While ROS levels decreased and CAT activity levels increased in the EGB intervention group compared with those in the model group, the difference in SOD activity between these two groups was not statistically significant (Fig. 5B and E-G). These results suggest that flavonoids from purslane have the potential to ameliorate oxidative stress damage in vitiligo.

PTF ameliorates oxidative stress impairment in B16F10 cells via the PI3K/AKT signaling axis. Western blot analysis demonstrated a significant reduction in the level of p-AKT/AKT protein in the H_2O_2 group compared with that in the control group. By contrast, the medium and high PTF groups and the EGB group exhibited elevated p-AKT/AKT protein levels compared with those in the H_2O_2 group. In particular, the

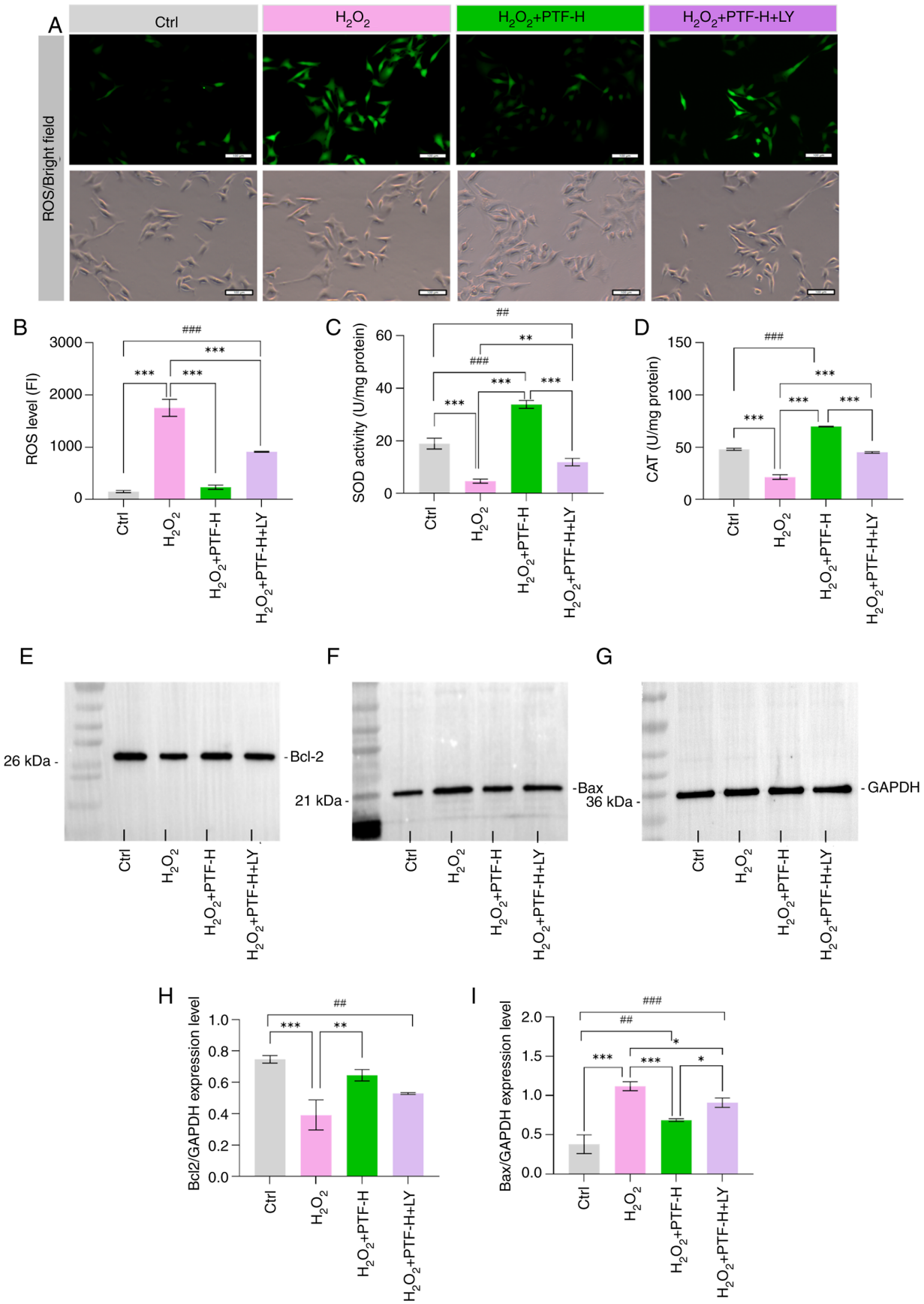

Figure 7. PI3K/AKT inhibitor attenuates the protective effect of PTF against H_2O_2-induced B16F10 cell injury. (A) Effects of different treatments on the ROS content of B16F10 cells (scale bar, 100 μm). Quantitative analysis of (B) ROS levels, (C) SOD activity and (D) CAT activity in the B16F10 cells. Western blot analysis of (E) Bcl-2, (F) Bax and (G) GAPDH internal control. Quantitative analysis of (H) Bcl-2 and (I) Bax protein expression. All data are presented as the mean ± standard error of the mean. $^{\#\#}$P<0.01 and $^{\#\#\#}$P<0.001 vs. the Ctrl group; *P<0.05, **P<0.01 and ***P<0.001 vs. the H_2O_2 group. PTF, purslane total flavonoids; H_2O_2, hydrogen peroxide; Ctrl, control; ROS, reactive oxygen species; SOD, superoxide dismutase; CAT, catalase; LY, LY294002; FI, fluorescence intensity.

high PTF group exhibited significantly higher p-AKT/AKT levels compared with those in the low PTF group. However, compared to the control group, the model group, the EGB intervention group and all PTF dose groups showed significant reductions (Fig. 6). No significant differences were observed in total AKT protein levels among the groups.

To investigate the involvement of the PI3K-AKT signaling pathway in the protective effect of PTF against H_2O_2-induced injury in B16F10 cells, the PI3K inhibitor LY294002 was used. Compared to the H_2O_2+PTF-H group, the LY294002 pretreatment group showed no significant difference in the expression level of Bcl-2, but a significant increase in Bax expression levels was observed (Fig. 7E-I). Furthermore, the PI3K inhibitor attenuated the protective effect of PTF against H_2O_2-induced oxidative damage in B16F10 cells. The ROS levels in the control and high PTF groups were significantly lower compared with those in the model group, whereas the SOD and CAT activities in the control and high PTF groups were significantly higher compared with those in the model group. The PI3K inhibitor significantly attenuated the changes in SOD and CAT activities compared with those in the high PTF group (Fig. 7A-D). These results suggest that PI3K/AKT signaling plays a key role in the protective effect of purslane on melanocytes subjected to oxidative stress.

Discussion

Purslane has a rich history of use in the treatment of various skin conditions, including vitiligo. However, the precise pharmacological mechanisms through which purslane ameliorates vitiligo remain elusive. In the present study, utilizing network pharmacology and molecular docking technology, seven core components, six core targets and one key signaling pathway of purslane in the treatment of vitiligo were identified. The key targets and pathway of the core components of purslane in the treatment of vitiligo were validated using a cell model. The findings indicate that the total flavonoids extracted from purslane exhibit therapeutic potential in vitiligo by mitigating oxidative stress-induced damage in melanocytes via the PI3K/AKT signaling pathway.

Vitiligo has been established to be an autoimmune disease, with known associations with various autoimmune conditions and hormone levels (8). Through network pharmacology analysis, the present study identified ESR1 and PTGS2 as potential regulators of vitiligo symptoms, which may act by modulating the molecular function of the 'hormone-mediated signaling pathway'. ESR1, a member of the NR3 subfamily of the nuclear hormone receptor family, plays a role in the proliferation, differentiation and homeostasis of melanocytes (38). It has been reported that elevated levels of estrogen in the serum are associated with increased skin pigmentation, and estrogen therapy is successful in the treatment of vitiligo (39). PTGS enzymes such as PTGS2, also known as cyclooxygenases, are essential for prostaglandin biosynthesis and function as dioxygenases and peroxidases. Studies have demonstrated that PTGS2 expression promotes the proliferation of keratinocytes following acute UV irradiation, leading to increased epidermal melanocyte and melanin production. This finding underscores an elevated functional activity of the melanocytes. (40,41). Collectively, these findings highlight the intricate relationship between hormone levels and skin pigmentation.

Patients with vitiligo typically present with hypopigmented macules and melanocyte dysfunction in the skin and mucosa (7). The pathogenesis of this condition remains incompletely understood, with proposed mechanisms encompassing genetic factors, melanocyte self-destruction, immune responses, oxidative stress and neurohumoral influences (42). Notably, the oxidative stress theory holds a central position in the pathogenesis of vitiligo. Elevated levels of ROS have been reported in the blood of patients with vitiligo compared with those in healthy individuals, with even higher levels observed in patients with active vitiligo relative to that in patients with stable vitiligo (43). These observations underscore the importance of oxidative stress in the pathophysiology of vitiligo. In the present study, network pharmacology analysis suggested that PTF may exert therapeutic effects on vitiligo by modulating the biological processes associated with 'cellular response to hypoxia', 'oxidoreductase activity' and 'positive regulation of reactive oxygen species metabolic process' through targeting AKT, TP53 and PPARG.

The loss of melanocytes is a key pathological feature of vitiligo, as they are the primary target cells in this condition. A recent study implicated genetic defects in melanocyte death, with ROS being pivotal in the pathogenesis of vitiligo (44). Oxidative stress disrupts the redox balance of cells, leading to the excessive production and inadequate clearance of ROS. Elevated ROS levels contribute to melanocyte destruction and cause structural and functional impairments to DNA, lipids, proteins and metabolites (45). In the present study, an oxidative damage model using B16F10 cells was used to evaluate the therapeutic potential of PTF in vitiligo and elucidate its underlying mechanism. The results demonstrated that PTF treatment significantly decreased H_2O_2-induced cytotoxicity in B16F10 cells, reduced ROS levels and increased the activity of SOD and CAT. Thus, PTF exhibits diverse biological functions, including cellular protection, that may be attributed to its robust antioxidant properties. Previous studies have highlighted the ability of PTF to ameliorate liver tissue injury and lipid peroxidation in non-alcoholic fatty liver disease models through the modulation of various markers including alanine aminotransferase, aspartate aminotransferase, triglycerides, fasting blood glucose, acetyl-CoA carboxylase, IL-6 and malondialdehyde, and by increasing carnitine palmitoyltransferase-1 and IL-10 levels and SOD activity (46). Collectively, these findings suggest that the therapeutic efficacy of purslane in vitiligo may be associated with the protective effects of total flavonoids against oxidative stress-induced damage in melanocytes.

In the present study, three flavonoids present in purslane, namely luteolin, kaempferol and quercetin, were indicated to play a pivotal role in the therapeutic management of vitiligo. Molecular docking studies revealed robust binding interactions between these flavonoids and the vitiligo therapeutic targets AKT1, MAPK1 and PPARG. AKT1 is a key signaling molecule involved in cell growth, division and apoptosis inhibition, which has been reported to phosphorylate β-catenin, leading to the activation of microphthalmia-associated transcription factor (MITF) and tyrosinases, thereby facilitating melanin synthesis (47). Melanocytes express three

PPAR isoforms, namely PPARα, PPARβ and PPARγ, and activators of PPARα and PPARγ have been demonstrated to inhibit melanocyte proliferation and enhance melanin secretion in a dose-dependent manner (48). Moreover, the MAPK signaling pathway is directly implicated in the regulation of the expression and activation of MITF, a key regulator of melanin biosynthesis (49). These findings suggest that the flavonoids luteolin, kaempferol and quercetin from purslane may mitigate melanocyte damage and apoptosis through modulation of AKT, MAPK1 and PPARG signaling pathways in melanocytes.

In the KEGG pathway enrichment analysis, 'PI3K-Akt signaling pathway' was identified as being pivotal in the treatment of vitiligo with PTF. Previous studies have indicated that in skin tissue, activation of this signaling pathway contributes to the maintenance of skin homeostasis (50) and protects melanocytes against apoptosis induced by oxidative stress (51). Notably, patients with vitiligo have been found to exhibit impaired activation of the PI3K/AKT pathway and reduced Nrf2 and phosphorylated PI3K levels in lesional skin cells, leading to the accumulation of oxidative species that heighten susceptibility to apoptosis and promote melanocyte death (43). However, purslane has been reported to protect hepatocytes through its anti-inflammatory and anti-oxidative properties, mediated by the PI3K/AKT/mTOR pathway (52). In addition, purslane extract has been shown to exert antioxidant and hypoglycemic effects via the PI3K/AKT pathway (53). In the present study, treatment with PTF was shown to activate the PI3K/AKT signaling pathway, as evidenced by significantly elevated levels of p-AKT in PTF-treated groups compared with the model group. Pre-treatment with the PI3K inhibitor LY294002 prior to PTF and H_2O_2 reduced the expression levels of Bcl-2 and increased the expression levels of Bax, indicating inhibition of the PI3K/AKT pathway by LY294002. In addition, the protective effects of PTF on B16F10 cells were markedly attenuated. These results underscore that PI3K/AKT signaling contributes to the protective effect of purslane against oxidative stress in melanocytes cells in vitiligo.

The present study has certain limitations; notably, the protective effect of each specific component of purslane against H_2O_2-induced oxidative damage in B16F10 cells was not verified. Furthermore, additional *in vivo* and clinical investigations are necessary to further corroborate the efficacy of purslane and its individual components in the treatment of skin lesions.

In summary, the present study used network pharmacology, molecular docking and *in vitro* assays to indicate that the total flavonoids of purslane may help to treat vitiligo via the mitigation of oxidative stress-induced damage in melanocytes through the PI3K/AKT signaling axis.

Acknowledgements

The authors would like to thank Professor Jinqiang Zhang and Professor Tao Zhou (both Resource Institute for Chinese and Ethnic Materia Medica of Guizhou University of Traditional Chinese Medicine, Guiyang, China) who provided assistance during the experimental process.

Funding

This study was supported by the National Natural Science Foundation of China (grant/award no. 82160908).

Availability of data and materials

The data generated in the present study may be requested from the corresponding author.

Authors' contributions

CW conceived and designed the study. XZ established the oxidative stress models and analyzed the cells using immunofluorescence and western blotting. LM detected the oxidative stress indicators. SL and XR collected and organized the data. XZ wrote the manuscript. CW and XZ confirm the authenticity of all the raw data. All authors read and approved the final version of the manuscript.

Ethics approval and consent to participate

Not applicable.

Patient consent for publication

Not applicable.

Competing interests

The authors declare that they have no competing interests.

References

1. Ezzedine K, Eleftheriadou V, Whitton M and van Geel N: Vitiligo. Lancet 386: 74-84, 2015.
2. Ezzedine K, Sheth V, Rodrigues M, Eleftheriadou V, Harris JE, Hamzavi IH and Pandya AG; Vitiligo Working Group: Vitiligo is not a cosmetic disease. J Am Acad Dermatol 73: 883-885, 2015.
3. Kruger C and Schallreuter KU: A review of the worldwide prevalence of vitiligo in children/adolescents and adults. Int J Dermatol 51: 1206-1212, 2012.
4. Bergqvist C and Ezzedine K: Vitiligo: A review. Dermatology 236: 571-592, 2020.
5. Kussainova A, Kassym L, Akhmetova A, Glushkova N, Sabirov U, Adilgozhina S, Tuleutayeva R and Semenova Y: Vitiligo and anxiety: A systematic review and meta-analysis. PLoS One 15: e0241445, 2020.
6. Ongenae K, Dierckxsens L, Brochez L, van Geel N and Naeyaert JM: Quality of life and stigmatization profile in a cohort of vitiligo patients and effect of the use of camouflage. Dermatology 210: 279-285, 2005.
7. Frisoli ML, Essien K and Harris JE: Vitiligo: Mechanisms of pathogenesis and treatment. Annu Rev Immunol 38: 621-648, 2020.
8. Khaitan BK and Sindhuja T: Autoimmunity in vitiligo: Therapeutic implications and opportunities. Autoimmun Rev 21: 102932, 2022.
9. Gao Y, Liang A, Fan X, Hu L, Hao F and Li Y: Safety research in traditional Chinese medicine: Methods, applications, and outlook. Engineering 5: 76-82, 2019.
10. Abdel-Malek ZA, Jordan C, Ho T, Upadhyay PR, Fleischer A and Hamzavi I: The enigma and challenges of vitiligo pathophysiology and treatment. Pigment Cell Melanoma Res 33: 778-787, 2020.
11. Rodrigues M, Ezzedine K, Hamzavi I, Pandya AG and Harris JE: New discoveries in the pathogenesis and classification of vitiligo. J Am Acad Dermatol 77: 1-13, 2017.

12. Li K, Xia T, Jiang Y, Wang N, Lai L, Xu S, Yue X and Xin H: A review on ethnopharmacology, phytochemistry, pharmacology and potential uses of *Portulaca oleracea* L. J Ethnopharmacol 319: 117211, 2024.
13. Lv WJ, Huang JY, Li SP, Gong XP, Sun JB, Mao W and Guo SN: *Portulaca oleracea* L. extracts alleviate 2,4-dinitrochlorobenzene-induced atopic dermatitis in mice. Front Nutr 9: 986943, 2022.
14. Zhou YX, Xin HL, Rahman K, Wang SJ, Peng C and Zhang H: *Portulaca oleracea* L.: A review of phytochemistry and pharmacological effects. Biomed Res Int 2015: 925631, 2015.
15. Ru J, Li P, Wang J, Zhou W, Li B, Huang C, Li P, Guo Z, Tao W, Yang Y, *et al*: TCMSP: A database of systems pharmacology for drug discovery from herbal medicines. J Cheminformatics 6: 13, 2014.
16. Zhang MQ and Wilkinson B: Drug discovery beyond the 'rule-of-five'. Curr Opin Biotech 18: 478-488, 2007.
17. Wang Y, Xiao J, Suzek TO, Zhang J, Wang J and Bryant SH: PubChem: A public information system for analyzing bioactivities of small molecules. Nucleic Acids Res 37: W623-W633, 2009.
18. Gfeller D, Michielin O and Zoete V: Shaping the interaction landscape of bioactive molecules. Bioinformatics 29: 3073-3079, 2013.
19. Stelzer G, Rosen N, Plaschkes I, Zimmerman S, Twik M, Fishilevich S, Stein TI, Nudel R, Lieder I, Mazor Y, *et al*: The GeneCards suite: From gene data mining to disease genome sequence analyses. Curr Protoc Bioinformatics 54: 1.30.1-1.30.33, 2016.
20. Bauer-Mehren A, Rautschka M, Sanz F and Furlong LI: DisGeNET: A Cytoscape plugin to visualize, integrate, search and analyze gene-disease networks. Bioinformatics 26: 2924-2926, 2010.
21. Bardou P, Mariette J, Escudie F, Djemiel C and Klopp C: jvenn: An interactive Venn diagram viewer. Bmc Bioinformatics 15: 293, 2014.
22. Shannon P, Markiel A, Ozier O, Baliga NS, Wang JT, Ramage D, Amin N, Schwikowski B and Ideker T: Cytoscape: A software environment for integrated models of biomolecular interaction networks. Genome Res 13: 2498-2504, 2003.
23. Tang Y, Li M, Wang J, Pan Y and Wu FX: CytoNCA: A cytoscape plugin for centrality analysis and evaluation of protein interaction networks. Biosystems 127: 67-72, 2015.
24. von Mering C, Huynen M, Jaeggi D, Schmidt S, Bork P and Snel B: STRING: A database of predicted functional associations between proteins. Nucleic Acids Res 31: 258-261, 2003.
25. Chin CH, Chen SH, Wu HH, Ho CW, Ko MT and Lin CY: cytoHubba: Identifying hub objects and sub-networks from complex interactome. Bmc Syst Biol 8 (Suppl 4): S11, 2014.
26. Dennis GJ, Sherman BT, Hosack DA, Yang J, Gao W, Lane HC and Lempicki RA: DAVID: Database for annotation, visualization, and integrated discovery. Genome Biol 4: P3, 2003.
27. Kanehisa M and Goto S: KEGG: Kyoto encyclopedia of genes and genomes. Nucleic Acids Res 28: 27-30, 2000.
28. Rigsby RE and Parker AB: Using the PyMOL application to reinforce visual understanding of protein structure. Biochem Mol Biol Edu 44: 433-437, 2016.
29. O'Boyle NM, Morley C and Hutchison GR: Pybel: A Python wrapper for the OpenBabel cheminformatics toolkit. Chem Cent J 2: 5, 2008.
30. Trott O and Olson AJ: AutoDock Vina: Improving the speed and accuracy of docking with a new scoring function, efficient optimization, and multithreading. J Comput Chem 31: 455-461, 2010.
31. Hseu YC, Chen XZ, Vudhya GY, Yen HR, Chuang JY and Yang HL: The Skin-whitening effects of ectoine via the suppression of alpha-MSH-stimulated melanogenesis and the activation of antioxidant Nrf2 pathways in UVA-irradiated keratinocytes. Antioxidants (Basel) 9: 63, 2020.
32. Yuan M, Chen L, Wang W, Qin D, Jia C, Liu C, Wang H, Zhu J, Guo Y, Zhou Y, *et al*: Emodin inhibits the proliferation and migration of B16F10 cells and induces their apoptosis. Transl Cancer Res 9: 6198-6205, 2020.
33. Baliyan S, Mukherjee R, Priyadarshini A, Vibhuti A, Gupta A, Pandey RP and Chang CM: Determination of antioxidants by DPPH radical scavenging activity and quantitative phytochemical analysis of ficus religiosa. Molecules 27: 1326, 2022.
34. Xiong J, Yang J, Yan K and Guo J: Ginsenoside Rk1 protects human melanocytes from H_2O_2-induced oxidative injury via regulation of the PI3K/AKT/Nrf2/HO-1 pathway. Mol Med Rep 24: 821, 2021.
35. Hseu YC, Vudhya GY, Wang LW, Zhang YZ, Chen XZ, Huang PJ, Yen HR and Yang HL: The in vitro and in vivo depigmenting activity of pterostilbene through induction of autophagy in melanocytes and inhibition of UVA-irradiated α-MSH in keratinocytes via Nrf2-mediated antioxidant pathways. Redox Biol 44: 102007, 2021.
36. Liu Y, Wang S, Jin G, Gao K, Wang S, Zhang X, Zhou K, Cai Y, Zhou X and Zhao Z: Network pharmacology-based study on the mechanism of ShenKang injection in diabetic kidney disease through Keap1/Nrf2/Ho-1 signaling pathway. Phytomedicine 118: 154915, 2023.
37. Busam KJ and Jungbluth AA: Melan-A, a new melanocytic differentiation marker. Adv Anat Pathol 6: 12-18, 1999.
38. Jin SY, Park HH, Li GZ, Lee HJ, Hong MS, Park HJ, Park HK, Seo JC, Yim SV, Chung JH and Lee MH: Association of estrogen receptor 1 intron 1 C/T polymorphism in Korean vitiligo patients. J Dermatol Sci 35: 181-186, 2004.
39. Jin SY, Park HH, Li GZ, Lee HJ, Hong MS, Park HJ, Park HK, Seo JC, Yim SV, Chung JH and Lee MH: Association of estrogen receptor 1 intron 1 C/T polymorphism in Korean vitiligo patients. J Dermatol Sci 35: 181-186, 2004.
40. Li M, Gao Y, Li C, Liu L, Li K, Gao L, Wang G, Zhang Z and Gao T: Association of COX2 functional polymorphisms and the risk of vitiligo in Chinese populations. J Dermatol Sci 53: 176-181, 2009.
41. Tripp CS, Blomme EA, Chinn KS, Hardy MM, LaCelle P and Pentland AP: Epidermal COX-2 induction following ultraviolet irradiation: Suggested mechanism for the role of COX-2 inhibition in photoprotection. J Invest Dermatol 121: 853-861, 2003.
42. LeWitt TM and Kundu RV: Vitiligo. JAMA Dermatol 157: 1136, 2021.
43. Kim H, Park CS and Lee AY: Reduced Nrf2 activation in PI3K phosphorylation-impaired vitiliginous keratinocytes increases susceptibility to ROS-generating chemical-induced apoptosis. Environ Toxicol 32: 2481-2491, 2017.
44. Xuan Y, Yang Y, Xiang L and Zhang C: The role of oxidative stress in the pathogenesis of vitiligo: A culprit for melanocyte death. Oxid Med Cell Longev 2022: 8498472, 2022.
45. Wang Y, Li S and Li C: Perspectives of new advances in the pathogenesis of vitiligo: From oxidative stress to autoimmunity. Med Sci Monitor 25: 1017-1023, 2019.
46. Farkhondeh T, Samarghandian S, Azimi-Nezhad M and Hozeifi S: The hepato-protective effects of *Portulaca oleracea* L. extract: Review. Curr Drug Discov Technol 16: 122-126, 2019.
47. Niu C, Yin L and Aisa HA: Novel furocoumarin derivatives stimulate melanogenesis in B16 melanoma cells by Up-regulation of MITF and TYR family via Akt/GSK3β/β -catenin signaling pathways. Int J Mol Sci 19: 746, 2018.
48. Kang HY, Chung E, Lee M, Cho Y and Kang WH: Expression and function of peroxisome proliferator-activated receptors in human melanocytes. Brit J Dermatol 150: 462-428, 2004.
49. Shin S, Ko J, Kim M, Song N and Park K: Morin induces melanogenesis via activation of MAPK signaling pathways in B16F10 mouse melanoma cells. Molecules 26: 2150, 2021.
50. Teng Y, Fan Y, Ma J, Lu W, Liu N, Chen Y, Pan W and Tao X: The PI3K/Akt pathway: Emerging roles in skin homeostasis and a group of Non-malignant skin disorders. Cells 10: 1219, 2021.
51. Denat L, Kadekaro AL, Marrot L, Leachman SA and Abdel-Malek ZA: Melanocytes as instigators and victims of oxidative stress. J Invest Dermatol 134: 1512-1518, 2014.
52. Guoyin Z, Hao P, Min L, Wei G, Zhe C and Changquan L: Antihepatocarcinoma Effect of *Portulaca oleracea* L. in Mice by PI3K/Akt/mTOR and Nrf2/HO-1/NF-κ B pathway. Evid-Based Compl Alt 2017: 8231358, 2017.
53. Lee JH, Park JE and Han JS: *Portulaca oleracea* L. extract reduces hyperglycemia via PI3k/Akt and AMPK pathways in the skeletal muscles of C57BL/Ksj-db/db mice. J Ethnopharmacol 260: 112973, 2020.